Shengbin Huang,[1,2] Yongfu Wang,[1] Xueqi Gan,[1,2] Du Fang,[1] Changjia Zhong,[1] Long Wu,[1] Gang Hu,[1] Alexander A. Sosunov,[3] Guy M. McKhann,[3] Haiyang Yu,[2] and Shirley ShiDu Yan[1]

Drp1-Mediated Mitochondrial Abnormalities Link to Synaptic Injury in Diabetes Model

Diabetes 2015;64:1728–1742 | DOI: 10.2337/db14-0758

Diabetes has adverse effects on the brain, especially the hippocampus, which is particularly susceptible to synaptic injury and cognitive dysfunction. The underlying mechanisms and strategies to rescue such injury and dysfunction are not well understood. Using a mouse model of type 2 diabetes (*db/db* mice) and a human neuronal cell line treated with high concentration of glucose, we demonstrate aberrant mitochondrial morphology, reduced ATP production, and impaired activity of complex I. These mitochondrial abnormalities are induced by imbalanced mitochondrial fusion and fission via a glycogen synthase kinase 3β (GSK3β)/dynamin-related protein-1 (Drp1)-dependent mechanism. Modulation of the Drp1 pathway or inhibition of GSK3β activity restores hippocampal long-term potentiation that is impaired in *db/db* mice. Our results point to a novel role for mitochondria in diabetes-induced synaptic impairment. Exploration of the mechanisms behind diabetes-induced synaptic deficit may provide a novel treatment for mitochondrial and synaptic injury in patients with diabetes.

Mitochondrial dysfunction, synaptic damage, and resultant impairment in cognitive function are pathological features of diabetes (1–11). Diabetes adversely affects the brain and confers increased risk for depression and dementia (3,12,13). In neurons, synaptic mitochondria are vital for maintenance of synaptic function and transmission through normal mitochondrial dynamics, distribution, and trafficking, as well as energy metabolism and synaptic calcium modulation. Imbalance in mitochondrial dynamics contributes to oxidative stress– and hyperglycemia-induced alterations in mitochondrial morphology and function (10,14,15). The molecular and cellular mechanisms regulating the precise distribution of mitochondria in neurons are poorly understood.

In addition to well-known adverse effects on the cardiovascular and peripheral nervous systems, the hippocampus is particularly susceptible to diabetes-induced episodic memory impairment (12) and synaptic plasticity deficits (5,7,8,11,16–20). For example, rats rendered diabetic by treatment with the pancreatic β-cell toxin streptozotocin (STZ) (a model of type 1 diabetes) exhibit spatial learning and memory impairment (5,8). Similar deficits have been reported in the insulin-resistant type 2 diabetes mouse model (7,8,16). Clinical investigations also documented impaired cognitive function in human subjects with type 1 (caused by insulin deficiency) as well as type 2 (mediated by insulin resistance) diabetes compared with age-matched nondiabetic subjects (21,22). In support of those findings, long-term potentiation (LTP) of synaptic transmission, believed to be a cellular mechanism of learning and memory, is impaired in the hippocampus of diabetic animal models (5,8,20). The decline of hippocampal LTP in diabetic individuals is partially due to increased corticosterone levels and/or impaired insulin signaling (8,19). Given that mitochondrial function is abnormal in many tissues negatively affected by diabetes and that mitochondria are important for maintenance of synaptic plasticity, as this organelle provides energy and regulates intrasynaptic metabolic homeostasis, we hypothesized that

[1]Department of Pharmacology & Toxicology and Higuchi Biosciences Center, School of Pharmacy, University of Kansas, Lawrence, KS
[2]State Key Laboratory of Oral Diseases, West China Hospital of Stomatology, Sichuan University, Chengdu, China
[3]Department of Neurosurgery, College of Physicians and Surgeons, Columbia University, New York, NY
Corresponding author: Shirley ShiDu Yan, shidu@ku.edu.

Received 12 May 2014 and accepted 15 November 2014.
This article contains Supplementary Data online at http://diabetes.diabetesjournals.org/lookup/suppl/doi:10.2337/db14-0758/-/DC1.

S.H. and Y.W. contributed equally to this work.

mitochondria-dependent mechanisms contribute importantly to diabetes-induced synaptic dysfunction such as hippocampal LTP deficit.

Mitochondria are dynamic organelles, which undergo continuous fission and fusion. Fission events are regulated by dynamin-related protein (Drp1), and fusion events are regulated by the large dynamin-related GTPases known as mitofusin (Mfn)1 and -2 as well as optic atrophy 1 (OPA1) (23–25). Alterations in mitochondrial dynamics significantly impact mitochondrial numbers and shape, respiratory enzyme activity, and ATP production. Imbalances of mitochondrial fission and fusion in diabetes result predominantly from upregulation of Drp1, which induces mitochondrial division and dysfunction (impaired respiration and ATP production) in a variety of cell types, including islet cells (26), hepatocytes (27), skeletal muscle cells (9,28), mononuclear blood cells (29), endothelial cells (30), and dorsal root ganglion neurons (15,31). Mitochondrial dysfunction is also suggested as a cause for development of insulin resistance in skeletal muscle cells and hyperglycemia in type 2 diabetes (32,33). Compared with other cell types, neurons are highly susceptible to mitochondrial dysfunction because neuronal transmission is regulated by energy homeostasis in synapses. In type 2 diabetes, hippocampal synaptic plasticity is widely believed to be impaired, but mechanisms for hippocampal mitochondrial damage and consequent neuronal dysfunction are unknown. The current study sought to elucidate how hippocampal mitochondria respond to diabetes-induced mitochondrial and synaptic alterations that result in synaptic injury.

RESEARCH DESIGN AND METHODS

Animals

These studies were approved by the Animal Care and Use Committee of University of Kansas-Lawrence in accordance with the National Institutes of Health guidelines for animal care. Leptin receptor heterozygous mice (animals are on C57BLKS background) were purchased from The Jackson Laboratory. Heterozygous *db/m* mice were crossed with each other to generate three genotypes of mice: wild-type mice, leptin receptor heterozygous mice (*db/m*), and homozygous leptin-deficiency mice (*db/db*). The genotype of offspring was identified by PCR using primers (forward, ACA AGA ACA AAA AGC CTG AAA CC, and reverse, CCA AAC TGA ACT ACA TCA AAC C) for genotyping as previously described (34). All *db/m* and *db/db* male mice used for the described experiments were 5–6 months of age unless otherwise stated. The investigators were blinded to the mouse genotype and treatment conditions in performing the immunoprecipitation, electron microscopy, and immunohistochemistry experiments.

SK Cell Culture and Transfections

Human SK-N-SH cells were cultured on 24-well culture plates at low density and incubated with DMEM with 10% FBS and 5.5 mmol/L D-glucose. Cells were then transfected with plasmids containing constitutively active forms of hemagglutinin–glycogen synthase kinase-3β (HA-GSK3β) (HA-GSK3β^{S9A}) or a dominant-negative form of GSK3β (HA-GSK^{K85A}) (Addgene), green fluorescence protein (GFP)-tagged wild-type Drp1 or Drp1^{K38A} (provided by Dr. Yi-Ren Hong, Kaohsiung Medical University Hospital, Taiwan), or empty control vectors (GFP or HA) using Lipofectamine 2000 (Invitrogen) according to the manufacturer's instructions. Forty-eight hours after transfection, cells were treated with indicated reagents and assessed for changes in mitochondrial morphology and function as well as molecular signaling pathways.

Electrophysiological Studies

Electrophysiological recordings were performed on coronal hippocampal slices (400 μm in thickness) as previously described (35). Hippocampal slices were recovered at 37°C for at least 1 h and then maintained in an interface chamber at 29°C and perfused with artificial cerebral spinal fluid (124 mmol/L NaCl, 4.4 mmol/L KC, 1 mmol/L Na_2HPO_4, 25 mmol/L $NaHCO_3$, 2 mmol/L $CaCl_2$, 2.0 mmol/L $MgSO_4$, and 10 mmol/L glucose) continuously bubbled with 95% O_2 and 5% CO_2. Field-excitatory postsynaptic potential (fEPSPs) was recorded from the CA1 region of the hippocampus by placing both the stimulating and the recording electrodes in the CA1 stratum radiatum. Basal synaptic transmission (input-output curve) was assayed by plotting the stimulus voltage (V) against slopes of fEPSP to generate input-output relations. A 30-min baseline recording was established using low-frequency stimulation (0.033 Hz; 0.1 ms impulse duration) and then adjusted intensity that induced fEPSPs with ~30% of the maximal fEPSP amplitude. LTP was induced by θ-burst stimulation (four pulses at 100 Hz, with the bursts repeated at 5 Hz, and each tetanus, including three 10-burst trains separated by 15 s). In experiments using inhibitors, drugs were continuously perfused over slices starting at least 1 h before LTP induction. Values of fEPSP slope were expressed as the percentage change relative to their mean baseline amplitude.

Drug Treatments

Drugs were prepared as stock solutions and were diluted to the final concentration immediately before use. Incubation of hippocampal slices with drugs was performed in either a recovery chamber or interface-recording chamber as needed. Drugs were added to culture plate wells. Final concentrations and sources of the drugs were as follows: 4-benzyl-2-methyl-1,2,4-thiadiazolidine-3,5-dione (TDZD8) (5 μmol/L; Sigma-Aldrich), mdivi-1 (10 μmol/L; Sigma-Aldrich), and glucose (50 mmol/L; Sigma-Aldrich). The final concentration of vehicle control DMSO was less than 0.5% in all experiments. For chronic in vivo administration of mdivi-1, the drug was dissolved in DMSO (10 or 25 mg/mL) as stock solution and further diluted in saline (DMSO: saline = 1:9) immediately before daily injection in diabetic or nondiabetic male mice at a dosage of 10 or 25 mg/kg i.p. Drug was administered once a day beginning at 19 weeks of age and continued for 2 weeks. The same

amount of DMSO dilution in saline was prepared and then administered to age-matched male nondiabetic and diabetic littermates as controls. One day after the end of treatment, animals were subjected to either electrophysiological studies or biochemistry assays.

Mitochondria Isolation

Brain mitochondria were isolated from whole brain cortex of mice or SK cultures as previously described (36). Briefly, samples were placed in 9 mL ice-cold mitochondria isolation buffer (225 mmol/L mannitol, 75 mmol/L sucrose, and 2 mmol/L K_2HPO_4 [pH 7.2]) and homogenized (10 strokes) using a Douce homogenizer (Kontes Glass Co.). Homogenate was centrifuged at 1,300*g* for 5 min at 4°C. The resultant supernatant was then centrifuged at 34,000*g* for 10 min after layering on 15% Percoll. After centrifugation, the homogenate was resuspended and incubated for 5 min on ice in 20 mL mitochondria isolation buffer with 0.02% digitonin and centrifuged at 8,000*g* for 10 min. The pellet was washed twice in 1.5 mL mitochondria isolation buffer and centrifuged again at 8,000*g* for 10 min. The final pellets were resuspended in 200 μL mitochondria isolation buffer. Total protein concentration of isolated mitochondria fraction was determined by Bradford protein assay (Bio-Rad Laboratory).

Immunoprecipitation and Immunoblotting Assays

For immunoprecipitation, hippocampal slices were lysed in nondenaturing lysis buffer containing 50 mmol/L Tris HCl (pH 8), 150 mmol/L NaCl, 1 mmol/L EDTA, 0.5% NP-40, and protease inhibitors (EMD Millipore). After centrifugation at 12,000*g* for 10 min at 4°C, the supernatant was precleaned with protein A/G-agarose beads (Thermo Scientific) for 2 h at 4°C, and 500 μg precleaned protein extracts was incubated with antibody to GSK3β or Drp1 for 16 h at 4°C. Precipitated complexes were washed in lysis buffer and bound proteins analyzed by immunoblots. For immunoblot experiments, hippocampal slices, cultured cells, or isolated mitochondrial/cytosol fractions were homogenized in cell lysis buffer (Cell Signaling), and then samples were separated in SDS-PAGE gels and transferred onto membranes. Polyclonal rabbit anti–phospho-GSK3β (Ser^9) (Cell Signaling), anti-GSK3β (3D10) (Cell Signaling), anti–phospho-Drp1 (Ser^{616}) (Cell Signaling), anti-Drp1 (Thermo Scientific), mouse anti–heat shock protein 60 (HSP60) (Enzo), and mouse anti–α-tubulin (Cell Signaling) were used as the primary antibodies. Binding sites of primary antibodies were visualized with horseradish peroxidase–conjugated anti-rabbit IgG antibody (Life Technology) or anti-mouse IgG antibody (Life Technology) followed by the addition of enhanced chemiluminescence substrate (GE Healthcare). Band relative optical density was determined by NIH ImageJ software (public domain) and normalized with α-tubulin levels.

Confocal and Electron Microscopy to Assess Mitochondrial Morphology

Brains were fixed by perfusion with 4% paraformaldehyde, and after additional fixation for 72 h at 4°C, coronal sections (25 μm) were cut with a Vibratome (Leica VTS1000). After blockade with 5% goat serum in PBS, slices were incubated with primary antibody (anti–superoxide dismutase 2 [SODII], Enzo Life Sciences; anti–cytochrome c oxidase [COXIV], Abcam; anti–microtubule-associated protein 2 [MAP2], Chemicon; or anti–Drp-1, BD Transduction Laboratories) overnight at 4°C. Secondary antibody (Alexa Fluor 488–conjugated goat anti-rabbit IgG and/or Alexa Fluor 594–conjugated goat anti-mouse IgG [Invitrogen]) was applied for 1 h at room temperature. Nuclei were stained by DRAQ5 (5 μmol/L; Cell Signaling) for 5 min at room temperature. Blocking serum and primary and secondary antibodies were applied in PBS with 0.3% Triton X-100. Brain sections incubated with preimmune serum or second antibody alone were used as negative controls. Mitochondria in cultured cells were visualized with MitoTracker red (100 nmol/L applied for 30 min at 37°C before fixation; Molecular Probes). Brain slices and cell cultures were examined under confocal microscope (Leica TCS SPE) with a 63 × 1.4 NA Apochrome objective (Carl Zeiss MicroImaging, Inc.) at 488 nm, 594 nm, or 543 nm wavelengths, respectively. For quantification of mitochondrial staining, four brain sections from each animal (five animals in each group) were randomly selected at different rostro-caudal hippocampal levels. More than twenty randomly selected hippocampal pyramidal neurons from each slice or SK cells in three independent experiments were used for quantification of mitochondrial length and density using MetaMorph software as we previously described (37). For analysis of electron microscopic images, we used our previously published method (35,38). Briefly, animals were perfused with 4% paraformaldehyde and 0.1% glutaraldehyde, and brains were fixed in the same fixative buffer overnight at 4°C. Small pieces of hippocampi were embedded in LR white medium (Electron Microscopy Laboratory). Ultra-thin sections were counterstained with uranyl acetate and examined using a JEOL 100S transmission electron microscope. Mitochondrial parameters such as major/minor axis length, perimeter, area, and density were measured using Metamorph software. The form factor was calculated as $\text{perimeter}^2/4\pi \times \text{area}$. The investigators were blinded to mouse genotype and treatment conditions in performing morphological analysis and immunohistochemical experiments.

Mitochondrial Respiration Complex Activity and ATP Measurement

Mitochondrial respiration complex activity was measured in hippocampi or in SK cell homogenates as previously described (37,39). Briefly, hippocampi or cultured cells were homogenized and sonicated in the isolation buffer containing 250 mmol/L sucrose; 20 mmol/L HEPES, pH 7.2; and 1 mmol/L EDTA. NADH-ubiquinone oxidoreductase (COXI) enzyme activity was determined in 25 mmol/L potassium buffer containing KCl, Tris-HCl ,and EDTA (pH 7.4). The change in absorbance was monitored at 340 nm wavelength every 20 s for 6 min using an Amersham

Biosciences Ultrospect 3100 pro spectrophotometer. For homogenized samples (50 μg protein), the oxidation of NADH was recorded for 3 min after the addition of 2 μg/mL antimycin, 5 mmol/L $MgCl_2$, 2 mmol/L KCN, and 65 μmol/L coenzymes Q1 to the assay mixture, and then 2 μg/mL rotenone was added to the mixture. The absorbance of samples was measured for another 3 min. Enzyme activities in complex II, complex III, complex IV, and citrate synthase activity were determined as previously described (37). We also determined ATP content in hippocampus using an ATP Bioluminescence Assay Kit (Roche) according to manufacturer's instructions with a Luminescence plate reader (Molecular Devices) with an integration time of 10 s.

Quantitative Real-Time PCR

Total RNA was extracted from hippocampal tissue using TRIzol reagent (Invitrogen Life Technologies, Carlsbad, CA) according to the manufacturer's protocol as described in our previous study (40). cDNA synthesis was performed using random hexamer primers and the TaqMan reverse transcription kit (Applied Biosystems, Foster City, CA). The TaqMan probes and primers Mm00802465_m1 were used for the standard TaqMan PCR procedures in the ABI Prism 7700HT Sequence Detection System (Applied Biosystems). Each treatment was performed in quadruplicate, and data were analyzed with the comparative Ct method (41) and normalized to GAPDH RNA of the corresponding sample.

Serum Insulin and Corticosterone Measurement

Animals were fasted for 6 h before obtaining blood samples. Blood samples were centrifuged at 2,500 rpm (4°C) for 5 min. Serum was then collected and stored at −80°C. ELISA kits for insulin and corticosterone were purchased from Abnova. Manufacturer's instructions for measurement of serum insulin and corticosterone concentrations were followed.

Data Analysis

Data are presented as means ± SEM. Statistics were analyzed using Statview software (SAS Institute). For comparison between the two groups, a two-tailed independent Student *t* test was used. For comparisons between multiple groups, one-way ANOVA was used followed by individual post hoc Fisher tests when applicable. $P < 0.05$ was considered statistically significant.

RESULTS

Alterations in Neuronal Mitochondrial Morphology and Function in Hippocampi of Diabetic Mice

To determine whether type 2 diabetes alters brain mitochondrial dynamics, architecture, and function, we examined the changes in hippocampus, which is particularly susceptible to adverse effects of diabetes (hippocampal damage results in episodic memory impairment [12] and synaptic plasticity deficits [5,7,8,11,16–20]). Using confocal microscopy and SODII (mitochondrial protein) immunostaining, we first examined mitochondrial morphology in CA1 neurons in *db/db* hippocampus compared with control *db/m* mice. SODII immunopositive mitochondrial density in *db/db* hippocampal neurons was significantly lower than that of *db/m* control mice (Fig. 1*A* and *B*). We next performed immunostaining with another mitochondrial marker, COXIV, to further examine the mitochondria density. As shown in Fig. 1*C–D*, the COXIV immunofluorescence intensity was significantly decreased in CA1 pyramidal neurons of *db/db* hippocampus compared with control *db/m* mice. To provide further evidence, we used electron microscopy to evaluate morphologic changes in hippocampal mitochondria (Fig. 1*E*) such as density, mitochondrial major axis length (mitochondrial length), the ratio of mitochondrial major axis length to minor axis length (mitochondrial width), and perimeters and area for calculation of form factor (indicating mitochondrial branching). The mitochondrial density (Fig. 1*F*), the length of mitochondria (major axes) (Fig. 1*G*), the ratio of mitochondrial length to width (Fig. 1*H*), and mitochondrial form factor (Fig. 1*I*) were significantly reduced within *db/db* hippocampus compared with *db/m* control hippocampus, suggesting decreased mitochondria branching and increased fragmentation in diabetic hippocampus. It has been reported that changes in mitochondrial numbers and shape can lead to impaired respiratory enzyme activity and energy production in tissue of diabetic mice (15,27,30,42–45). Therefore, we next evaluated hippocampal mitochondrial function by measuring key enzyme activity associated with respiratory chain and ATP levels. Complex I activity was significantly reduced in *db/db* hippocampal mitochondria compared with age-matched nondiabetic littermates (Fig. 1*J*); complex II and IV activities were unchanged (Supplementary Fig. 1). Similarly, hippocampal ATP abundance in *db/db* mice was significantly lower than in *db/m* control mice (Fig. 1*K*). Our data demonstrate that mitochondrial shape changes were paralleled with decreases of mitochondrial respiratory enzyme activity and ATP abundance in diabetic hippocampus.

Given that imbalance of mitochondrial fission and fusion plays a critical role in maintenance of morphology, distribution, and function, we next investigated whether mitochondrial dynamics properties were altered in diabetes. Immunoblotting of hippocampal homogenates revealed that levels of the mitochondrial fission protein Drp1 were increased in diabetic mice (Fig. 1*L* and *O*), but levels of mitochondrial fusion proteins Mfn2 and OPA1 in diabetic *db/db* hippocampus were not significantly different from *db/m* control levels ($P > 0.05$ *db/m* vs. *db/db*) (Supplementary Fig. 2*A*). While the effect of Drp1 upregulation/activation on mitochondrial fusion/fission is sometimes still controversial, accumulated evidence suggests that the Drp1-dependent mitochondrial elongation or fragmentation is closely associated with its phosphorylation status at different amino acid sites. Among those phosphorylated residues, phosphorylation of Ser^{616} was reported to be associated with mitochondrial fission (46). Indeed, we observed an increase in Ser^{616} phosphorylation in parallel with an increase in total Drp1

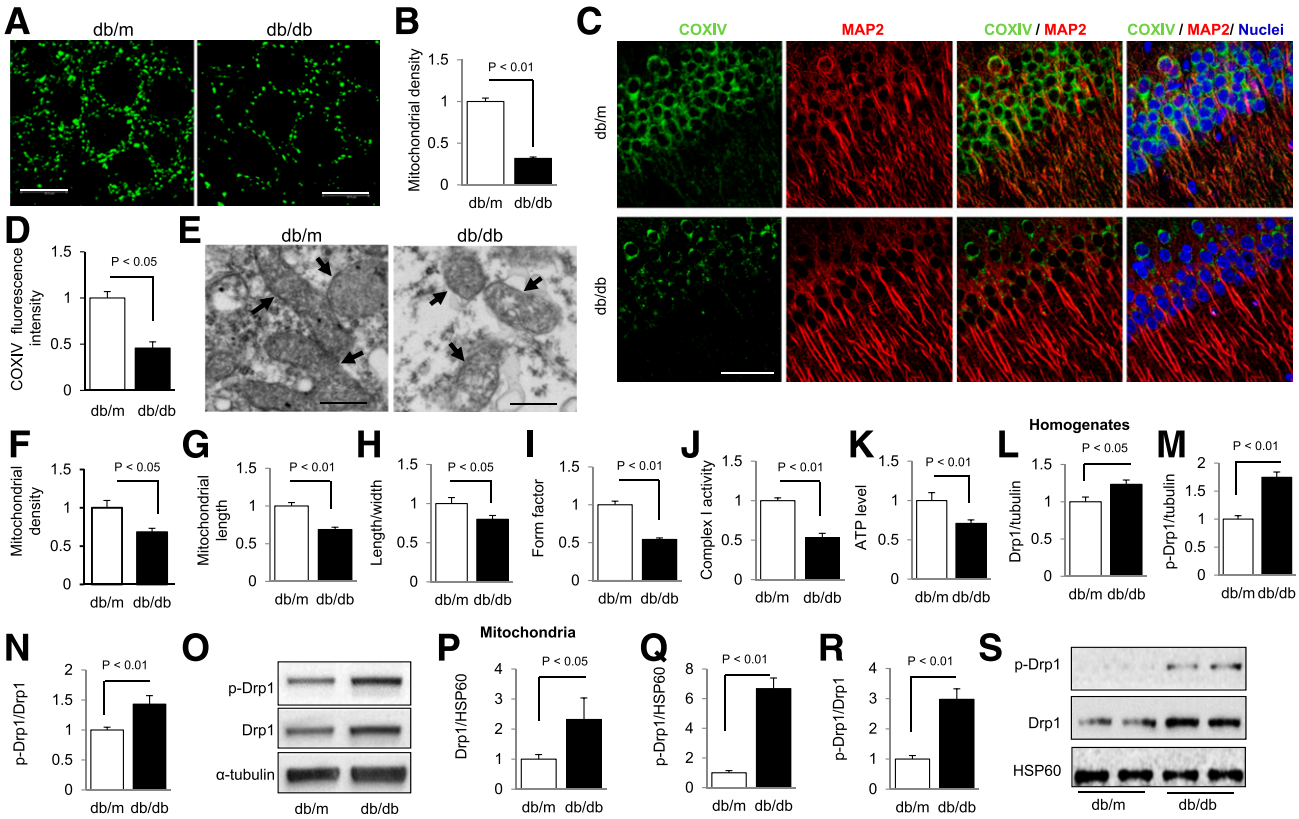

Figure 1—Mitochondrial alterations in hippocampus of *db/db* mice. *A*: Representative images of SODII staining of hippocampal neurons from *db/m* (left) or *db/db* (right) mice. *B*: Measurement of mitochondrial density (data presented as the fold increase of the percentage of area occupied by mitochondria in cell body) using MetaMorph software. *C*: Representative images for COXIV (green) and MAP2 (red) staining in hippocampal pyramidal neurons from *db/m* and *db/db* brains. Nuclei were stained by DRAQ5 as shown in blue signals. *D*: Quantification of immunofluorescence intensity of COXIV in hippocampal pyramidal neurons from *db/m* and *db/db* mice. *E*: Electron microscope images of mitochondria (indicated by arrows) from *db/m* and *db/db* hippocampus. Measurements of mitochondrial density (*F*), length (*G*), ratio of length to width (*H*), and form factor (*I*) from electron microscope images. *J* and *K*: Enzymatic activity of complex I (*J*) and ATP levels (*K*). *L*–*O*: Densitometry of immunoreactive bands for Drp1 (*L*) and Ser^{616} phosphorylated Drp1 (p-Drp1) (*M*) that normalized to α-tubulin in hippocampus homogenates of indicated groups and phosphorylated Drp1/Drp1 (*N*). *O*: Representative immunoreactive bands for Drp1, phosphorylated Drp1, and α-tubulin. *P*–*S*: Densitometry of immunoreactive bands for Drp1 (*P*) and Ser^{616} phosphorylated Drp1 (*Q*) relative to HSP60 (mitochondrial marker) in brain mitochondrial fractions isolated from *db/m* and *db/db* mice. The level of phosphorylated Drp1/Drp1 was increased in *db/db* brain mitochondria (*R*). *S*: Representative immunoreactive bands for Drp1, phosphorylated Drp1, and HSP60 in mitochondrial fractions in groups of mice as indicated. Data are presented as fold increase relative to *db/m* mice. Scale bar = 10 or 50 μm in *A* or *C* for confocal images, respectively, and 500 nm for electron microscope images in *E*. *N* = 6–8 animals per group.

expression in hippocampus of *db/db* mice (Fig. 1*M*–*O*). An elevated level of Drp1 was found in diabetes-affected CA1 neurons (Supplementary Fig. 2*B* and *C*). Furthermore, quantitative real-time PCR assay revealed that the gene expression of Drp1 was increased~1.3 fold in *db/db* animals compared with that of *db/m* controls (Supplementary Fig. 2*D*). Because the mitochondrial translocation of phosphorylated Drp1 at Ser^{616} is necessary to promote fission (46), we then determined the levels of Drp1 in mitochondria. Immunoblotting of the isolated brain mitochondria displayed increased levels of Drp1 (Fig. 1*P* and *S*) and of phosphorylation of Drp1 (Fig. 1*Q*–*S*) in diabetes-affected brain compared with *db/m* controls. These results suggest increased mitochondrial fission in diabetic mice, which may subsequently impair mitochondrial morphology and function.

Mitochondria Fission Is Increased in Diabetes Cell Culture Model

Next, using a human neuronal SK cell line, we elucidated the role of Drp1 in mitochondrial alterations under diabetic conditions. We first investigated whether there was an increased mitochondrial translocation of Drp1 in diabetic conditions. Treatment with high glucose (50 mmol/L D-glucose for 1 h) lowered the cytosol Drp1 level (Fig. 2*A*) but increased mitochondrial Drp1 protein (Fig. 2*B*) compared with that in control cells treated with L-glucose, a nonmetabolizable form of glucose (data not shown). In addition, immunostaining of Drp1 demonstrated localization of Drp1 in mitochondria treated with high glucose as demonstrated by overlaying a Drp1 image with the mitochondrial marker MitoTracker (Fig. 2*C*). These data suggested that high-glucose exposure

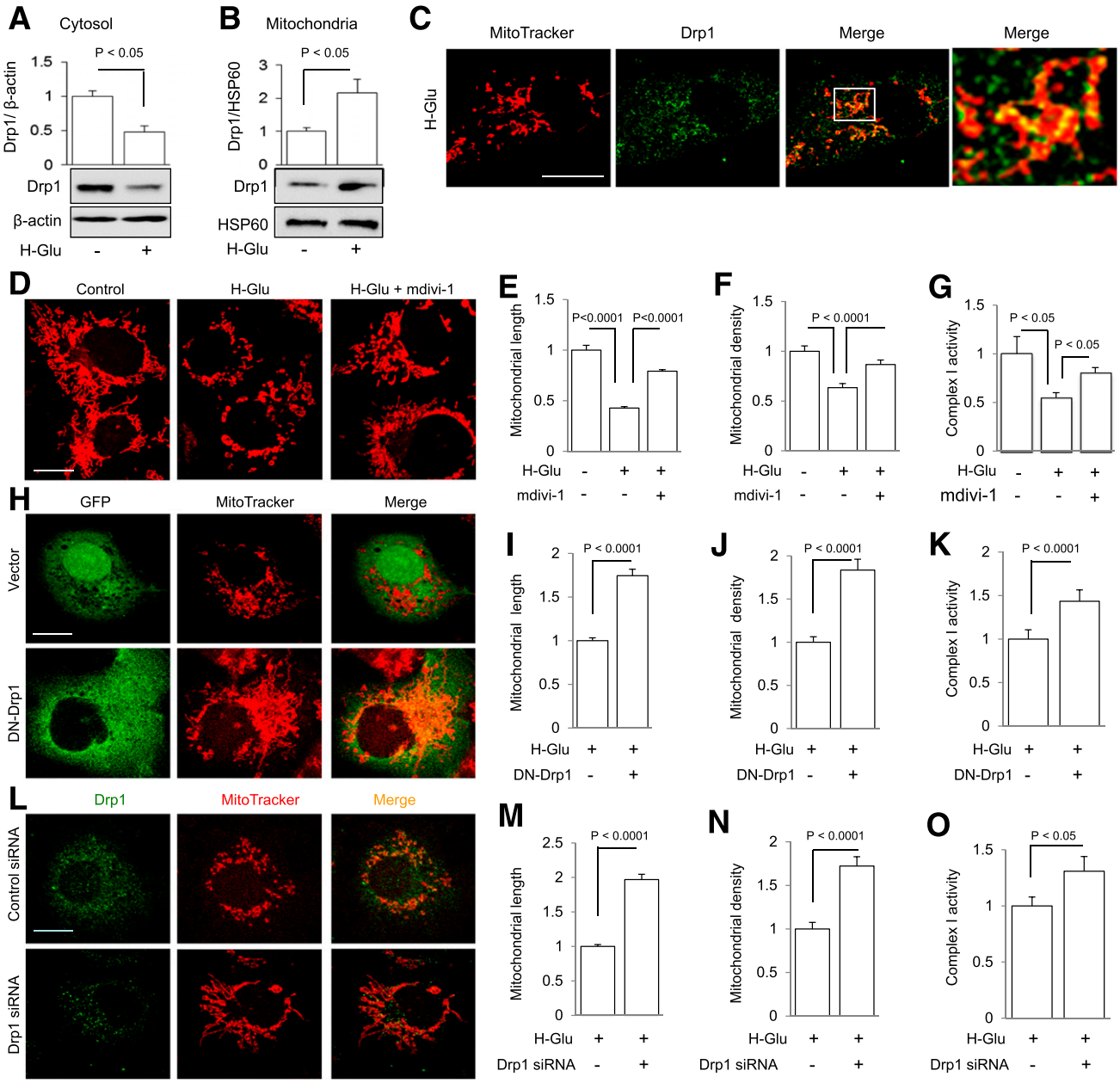

Figure 2—Drp1 activation is responsible for mitochondrial morphology changes in human neuronal SK cells under high-glucose conditions. *A* and *B*: The levels of Drp1 in cytosol (*A*) or in mitochondrial fraction (*B*) of indicated groups were quantified using ImageJ software. *C*: Representative images of MitoTracker red (100 nmol/L MitoTracker red was added to cultures 30 min prior to fixation), Drp1 (green), merged images, and an enlarged magnification (as indicated in white rectangle of merge image). Colocalization of Drp1 with MitoTracker red is shown in yellow. The rightmost image is an enlargement of the boxed area as shown in the merged image. *D*: Representative images for MitoTracker red staining to show mitochondrial morphology in the indicated groups of cells. *E–G*: Measurement of mitochondrial length (*E*) and density (*F*) using MetaMorph software and enzymatic activity of complex I (*G*) with mdivi-1 (+) or vehicle (-) treatment. *H*: SK cells were transfected with construct encoding GFP vector alone (labeled as vector) or GFP-tagged Drp1^{K38A} (DN-Drp1) and stained with MitoTracker red (100 nmol/L MitoTracker red was added to cultures 30 min prior to fixation). Representative images for GFP (left), MitoTracker red (middle), and the two merged (right) from SK cells transfected with the empty GFP vector (upper panel) or GFP-Drp1^{K38A} (DN-Drp1) (lower panel) construct in the presence of high-glucose concentration (50 mmol/L). *I–K*: Measurement of mitochondrial length (*I*), density (*J*), and complex I activity (*K*) in cells transfected with vector alone (-) or DN-Drp1 (+). *L*: SK cells were transfected with Drp1 siRNA or control siRNA, and then mitochondrial morphology was examined under confocal microscopy. Representative images for Drp1 immunostaining (left) (green), MitoTracker red (middle), and the two merged (right) from cells treated with control siRNA (upper panel) or Drp1 siRNA (lower panel). *M–O*: Measurement of mitochondrial length (*M*), density (*N*), and complex I activity (*O*) in cells transfected with control siRNA (-) or Drp1 siRNA (+). Data are presented as fold increase relative to control siRNA-treated cells in the presence of high glucose. Scale bar = 10 μm. $N \geq 20$ cells per group from two independent experiments. Mdivi-1, 10 μmol/L. H-GLu (-) or (+) denotes culture medium containing 5.5 mmol/L (-) or 50 mmol/L (+).

induce mitochondrial translocation of Drp1 in cultured SK cells, which was similar to what we observed in the type 2 diabetes–affected animal brain (Fig. 1).

We also examined whether the high-glucose treatment in vitro induced mitochondrial defects comparable with those we demonstrated in vivo. Here, we observed decreased mitochondrial length (Fig. 2*D* and *E*), density (Fig. 2*D* and *F*), and complex I enzyme activity (Fig. 2*D* and *G*) in SK cells subjected to high-glucose conditions (50 mmol/L) for 1 h. Notably, the nonmetabolizable sugar, mannitol or L-glucose, used as an osmotic control, did not induce any noticeable alterations, meaning that the mitochondrial changes were specifically dependent on the high glucose–induced diabetic insult (Supplementary Fig. 3). Importantly, high glucose–induced deleterious effects were significantly prevented by pretreatment with mdivi-1 (10 μmol/L), an inhibitor of Drp1 activity (47) (Fig. 2*D–G*). For determination of a specific effect of Drp1 on mitochondria pathology, cells were transfected with inactivated Drp1 and evaluated for mitochondria morphology and function under diabetic conditions. In this case, we transfected SK cells with GFP-tagged dominant negative mutant Drp1 (DN-Drp1) to determine the effect of DN-Drp1 on high glucose–induced mitochondrial morphology changes. Compared with the control vector–transfected cells, inactivation of Drp1 significantly preserved mitochondria against deleterious effects of high-glucose treatment (Fig. 2*H–K*). Additionally, knockdown of Drp1 with small interfering RNA (siRNA) protected mitochondrial morphology, dynamics, and function from adverse effects of high-glucose exposure (Fig. 2*L-O*). No significant difference of mitochondrial dynamics and function were found in cells transfected with DN-Drp1 (Supplementary Fig. 4*A–C*) or Drp1 siRNA (Supplementary Fig. 4*D–F*) compared with cells transfected with GFP vector alone or control siRNA under the vehicle-treated normal glucose condition. These results indicate that Drp1 potentiates neuronal mitochondria abnormalities under diabetic conditions in vitro as well.

GSK3β Directly Regulates Drp1 in Diabetic Condition

It is known that GSK3β is activated in *db/db* mice owing to dephosphorylation on Ser^9 residue (48–50) and it can use Drp1 as one of its substrates in an in vitro system (51–53). We thereby evaluated whether GSK3β could directly regulate Drp1 in diabetes-affected brain. Immunoprecipitation of Drp1 followed by immunoblotting with GSK3β showed a GSK3β immunoreactive band. Conversely, immunoprecipitation of GSK3β showed Drp1 immunoreactive bands (Fig. 3*A*), suggesting the formation of a complex of Drp1 with GSK3β in a mouse model of type 2 diabetes. GSK3β is a serine/threonine kinase, and phosphorylation on Ser^9 residue (p-ser9 GSK3β) inactivates it (50). Most interestingly, p-ser9 GSK3β levels are decreased in both diabetic human subjects and rodent models of diabetes (48,49), indicating increased GSK3β activation. In the current study, we also observed an increased GSK3β activation (reduced levels of p-ser9 GSK3β) in *db/db* mice compared with *db/m* control littermates (Fig. 3*B*). Treatment with TDZD8 (5 μmol/L for 1 h), an inhibitor of GSK3β (54), resulted in a significant increase of p-ser9 GSK3β levels in *db/db* hippocampus (Fig. 3*B*), suggesting that TDZD8 treatment may be sufficient to inhibit GSK3β activation in diabetic hippocampal tissue. Further, in the presence of TDZD8, we observed a decreased Drp1 protein expression ($P < 0.001$, vehicle-perfused *db/db* hippocampal slices vs. TDZD8-perfused *db/db* slices [Fig. 3*C*]) and decreased Drp1 Ser^{616} phosphorylation ($P < 0.05$, vehicle-perfused *db/db* hippocampal slices vs. TDZD8-perfused *db/db* slices [Fig. 3*C* and *D*]) in *db/db* mouse hippocampal tissue.

To investigate direct effect of GSK3β on Drp1-mediated mitochondrial alterations under diabetic conditions, human neuronal SK cells were treated with GSK3β inhibitor TDZD8 or transfected with a dominant negative form of GSK3β (DN-GSK3β) in the presence of high glucose. Clearly, pharmacological blockade (Fig. 3*E–G*) or genetic inhibition of GSK3β (Fig. 3*H–I*) prevented high glucose–induced Drp1 changes. In addition, transfection of SK cells with the $GSK3β^{S9A}$ (constitutively active form of GSK3β) resulted in increased Drp1 expression and its phosphorylation (Fig. 3*J* and *K*). Additionally, we performed triple immunostaining for mitochondria (red), Drp1 (green), and GSK3β (blue) to determine whether there was a colocalization of GSK3β and Drp1 in mitochondria under a diabetic condition. As shown in Fig. 3*L*, the high-glucose treatment induced a colocalization (white) of GSK3β/Drp1 within mitochondria in SK cultures.

Since Drp1 plays a key role in maintenance of mitochondrial structure and function and is directly regulated by GSK3β, we next tried to determine whether modulation of GSK3β causes changes in mitochondrial morphology under diabetic conditions. Pharmacological blockade of GSK3β with TDZD8 significantly suppressed mitochondrial fission (Fig. 4*A* and *B*) and increased mitochondrial density (Fig. 4*A* and *C*) and complex I activity (Fig. 4*D*) in the presence of high-glucose treatment. Genetic inactivation with DN-GSK3β also preserved mitochondria against high-glucose insult (Fig. 4*E–H*). Neither pharmacological (Supplementary Fig. 4*G–I*) nor genetic (Supplementary Fig. 4*J–L*) inhibition of GSK3β had any significant effect on the mitochondrial morphology and function in vehicle-treated cells. As expected, activation of GSK3β by transfecting cells with $GSK3β^{S9A}$ elicited mitochondrial impairments (Fig. 4*I–L*). These results demonstrate that GSK3β-Drp1 interaction mediates mitochondrial alteration under diabetic condition.

To validate that GSK3β acts as an upstream Drp1 signaling in diabetic conditions, we cotransfected SK cells with $GSK3β^{S9A}$ with and without DN-Drp1 plasmids or DN-GSK3β with or without Drp1 plasmids. Transfection with DN-Drp1 prevented effects of $GSK3β^{S9A}$-mediated alterations in mitochondrial morphology and complex I enzyme activity (Fig. 5*A–D*). However, transfection with

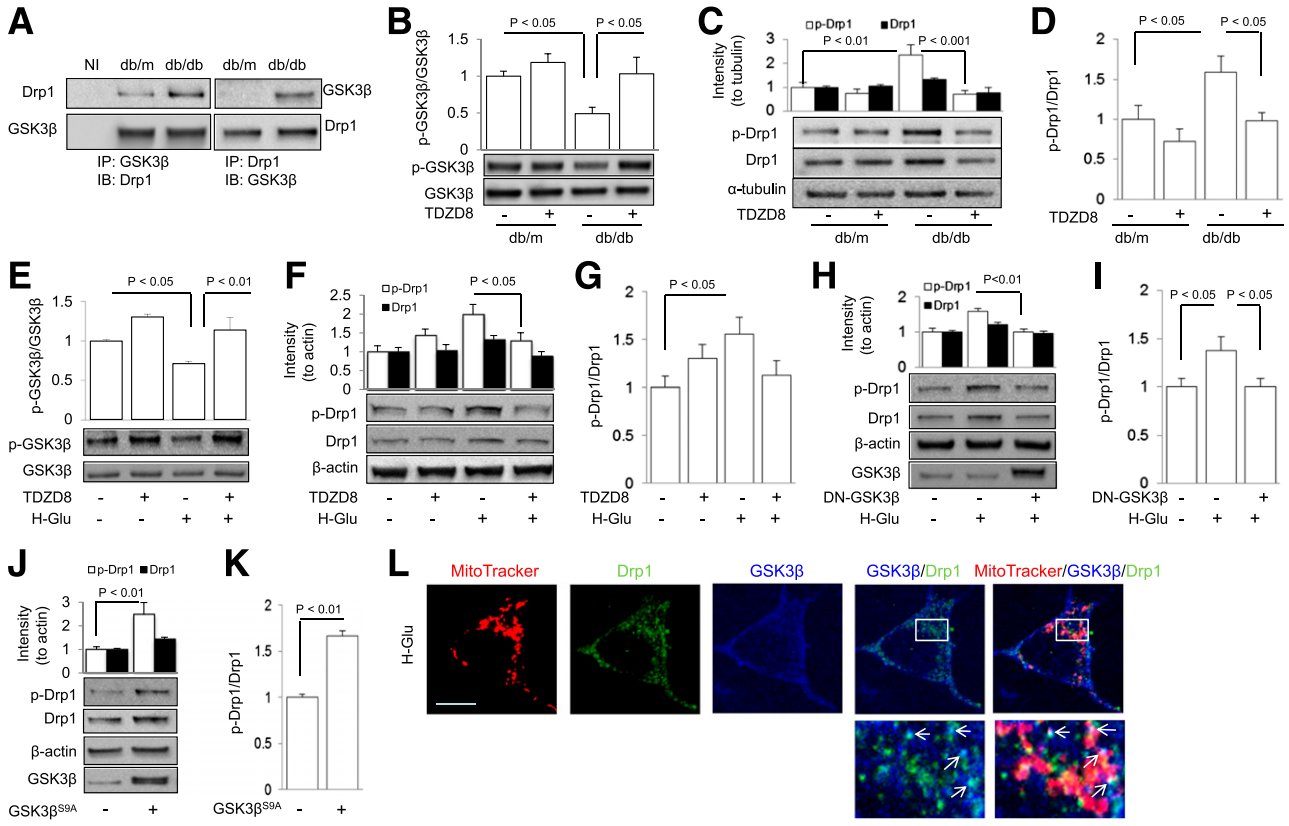

Figure 3—GSK3β/Drp1 interaction in diabetic hippocampus and SK cell line. *A*: Densitometry of immunoreactive bands. GSK3β (upper right panel) or Drp1 (upper left panel) after immunoprecipitation (IP) of Drp1 or GSK3β, respectively. Lower panels are protein input controls. NI, nonimmune IgG. *B*: Densitometry of immunoreactive bands for Ser^{9} phosphorylated GSK3β (p-GSK3β) relative to GSK3β in hippocampus homogenates of the indicated groups. The representative immunoblots for phosphorylated GSK3β or GSK3β are shown in the lower panel. *C* and *D*: Quantification of the density of immunoreactive Drp1 and phosphorylated Drp1 bands normalized to α-tubulin (*C*). The lower panel of *C* shows representative immunoblots for phosphorylated Drp1, Drp-1, and α-tubulin in hippocampal homogenates from *db/m* and *db/db* with (+) or without (-) GSK3β inhibitor TDZD8. The phosphorylated Drp1/Drp1 was calculated (*D*) from hippocampal slices with or without GSK3β inhibitor TDZD8 (5 μmol/L, treated for 1 h). *E*–*G*: Densitometry of immunoreactive bands for p-GSK3β (*E*), Drp1 and phosphorylated Drp1 relative to β-actin (*F*), and ratio of phosphorylated Drp1 to Drp1 (*G*) in the SK cells with (+) or without (-) TDZD8 treatment in the presence of high glucose (+) or culture medium (-). *H* and *I*: SK cells transfected with dominant negative form of GSK3β (DN-GSK3β) changed phosphorylated Drp1 and Drp1 expression levels (*H*) and phosphorylated Drp1–to–Drp1 ratio (*I*). The lower panel of *H* shows representative immunoblots for the indicated protein in vector (-) or HA-DN-GSK3β–transfected (+) SK cells in the presence of high-glucose levels (+) or vehicle (-). *J* and *K*: SK cells transfected with constitutively active mutant of GSK3β (GSK3β^{S9A}) changed phosphorylated Drp1 and Drp1 expression levels relative to β-actin (*J*) and phosphorylated Drp1–to–Drp1 ratio (*K*) in indicated groups. The lower panel of *J* shows representative immunoblots for the indicated protein in vector (-) or GSK3β^{S9A}-transfected (+) SK cells. *L*: Representative images of triple immunostaining for mitochondria (MitoTracker red), Drp1 (green), and GSK3β (blue) in high glucose (H-Glu)–treated SK cells. The enlarged box area was demonstrated in the lower panel. Arrows pointing to spots denote colocalization of Drp1 with GSK3β and MitoTracker red. Data are presented as fold increase relative to vehicle-treated controls; N = 4–6 animals per group or culture wells from three independent experiments. Scale bar = 10 μm. H-GLu (-) or (+) denotes culture medium containing 5.5 mmol/L (-) or 50 mmol/L (+). (-) indicates the vehicle treatment or control vector transfection and (+) indicates the presence of the indicated drug treatment or indicated construct transfection. IB, immunoblotting.

DN-GSK3β did not completely restore Drp1 transfection–induced mitochondria impairments (Fig. 5*E*–*H*). These results indicate that Drp1 was required for GSK3β activation–mediated mitochondrial dysfunction. In addition, suppressing Drp1 did not change GSK3β activation that was induced by either high-glucose treatment in cells or type 2 diabetic hippocampus. As showed in Supplementary Fig. 5*A* and *B*, reduced GSK3β phosphorylation in cells with high-glucose treatment was not restored by modulation of Drp1 via transfection with DN-Drp1 or Drp1 siRNA. Similarly, administration of mdivi-1, a potent cell-permeable inhibitor of Drp1 (47), to *db/db* mice failed to alter levels of p-ser9 GSK3β ($P > 0.05$, vehicle-treated *db/db* vs. mdivi-1 treated *db/db* hippocampal slices [Supplementary Fig. 5*C*]). These data suggest that GSK3β is a likely upstream signaling molecule that controls Drp1 activity under diabetic conditions.

Mitochondrial Impairment Is Responsible for Synaptic Plasticity Deficit

We further sought to investigate the role of Drp1 in mediating mitochondrial degeneration and energy supply

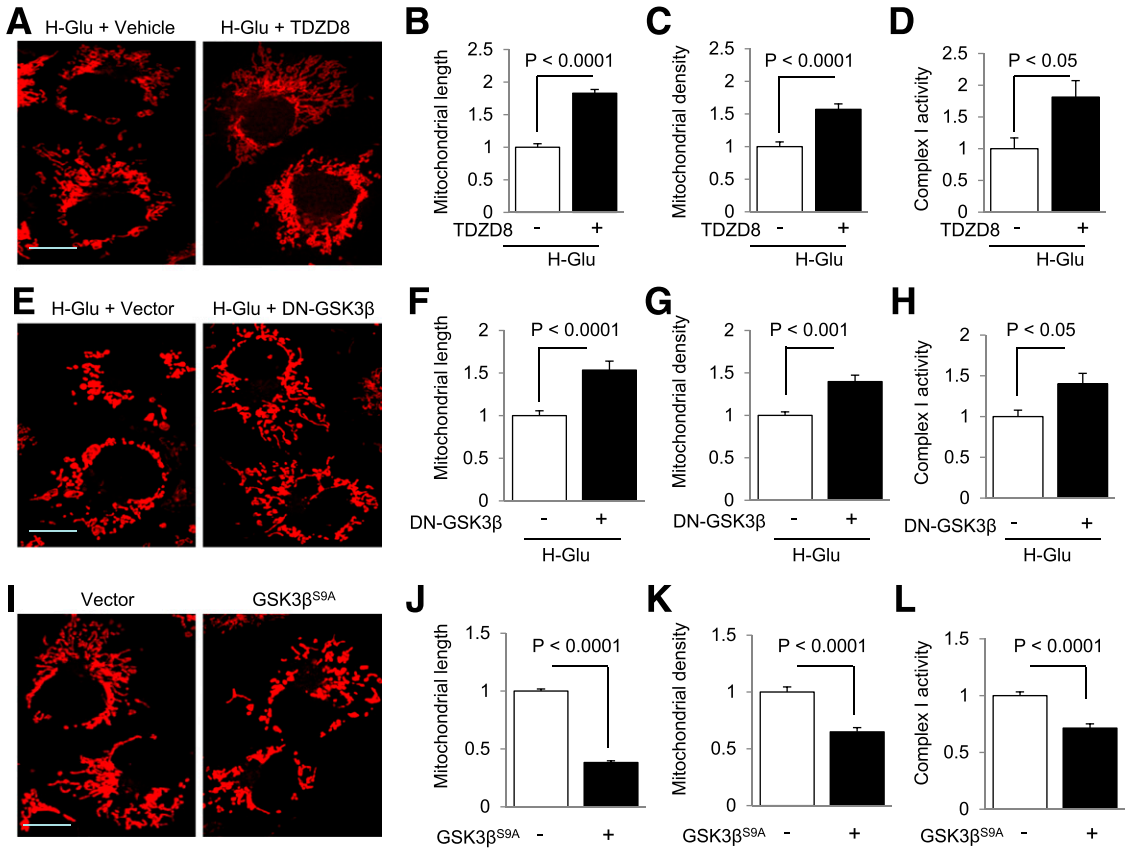

Figure 4—Inactivation of GSK3β prevents high glucose–induced mitochondrial morphology alterations and functional deficit. *A–D*: Representative images of MitoTracker red staining (*A*) and measurements of mitochondrial length (*B*), density (*C*), and complex I activity (*D*) with (+) or without (-) TDZD8 treatment (5 μmol/L for 1 h) in human SK cells under high-glucose conditions. *E–H*: Representative images of MitoTracker red staining (*E*) and quantification of mitochondrial length (*F*), density (*G*), and complex I activity (*H*) with empty (-) or HA-DN-GSK3β (+) plasmid transfection in human SK cells under high-glucose conditions. *I–L*: Representative images of MitoTracker staining (*I*) and quantification of mitochondrial length (*J*), density (*K*), and complex I activity (*L*) with empty (-) or HA-GSK3β^{S9A} (+) plasmid transfection in human SK cells under normal glucose conditions. Data are presented as fold increase relative to vehicle-treated SK cells. $N \geq 20$ cells per group from three independent experiments. Scale bar = 10 μm. H-GLu (-) or (+) denotes culture medium containing 5.5 mmol/L (-) or 50 mmol/L (+). (-) Indicates the vehicle treatment or control construct transfection and (+) indicates the presence of the indicated drug treatment or indicated construct transfection.

deficiency in diabetes-affected hippocampus by assessing whether suppression of Drp1 expression and activity in diabetic brain would have favorable effects. Treatment with Drp1 inhibitor mdivi-1 (25 mg/kg or 10 mg/kg once daily for 2 weeks) resulted in significantly increased mitochondrial content (Fig. 6*A* and *B*), complex I enzymatic activity (Fig. 6*C*), and ATP levels (Fig. 6*D*) in *db/db* mouse hippocampus. When the same mdivi-1 treatment was administered to *db/m* control animals, we found no significant changes in mitochondrial density (Fig. 6*A* and *B*), complex I activity (Fig. 6*C*), or ATP levels (Fig. 6*D*). Electron microscopy confirmed that mdivi-1 treatment (10 mg/kg) significantly preserved mitochondrial morphology by maintaining mitochondrial length and shape (Fig. 6*E–I*).

Because mitochondrial morphology and function are crucial for synaptic plasticity and function (55–58), we next investigated mitochondria-dependent mechanisms of synaptic plasticity in hippocampus of the *db/db* mouse model of type 2 diabetes. Using electrophysiological analysis, we observed reduced LTP (Fig. 7*C*), whereas basal neuronal transmission (input-output relationship [Fig. 7*A*]) or short-term plasticity (pair-pulse facilitation [Fig. 7*B*]) was not changed in *db/db* hippocampus. Treatment with mdivi-1 significantly reversed the decline in hippocampal LTP from diabetic hippocampus ($P < 0.05$, mdivi-1–treated *db/db* mice vs. vehicle-treated *db/db* hippocampal slices [Fig. 7*G* and *H*]) without changes in basic neuronal transmission or pair-pulse facilitation (Fig. 7*E* and *F*). The treatment of nondiabetic *db/m* mice with mdivi-1 did not significantly affect hippocampal LTP (Fig. 7*D* and *H*), which was coincident with the unaffected mitochondrial structure and function (Fig. 6). Taken together, these results indicate a protective effect of inhibition of diabetes-induced Drp1 activation on synaptic dysfunction.

Given that GSK3β activation modulated Drp1 signaling, we next evaluated whether treatment of hippocampus slices with GSK3β inhibitor TDZD8 or LiCl (4 mmol/L) recapitulated the protective effects of mdivi-1 on synaptic function in vivo. Indeed, inhibition of GSK3β significantly protected hippocampus LTP against diabetes insult

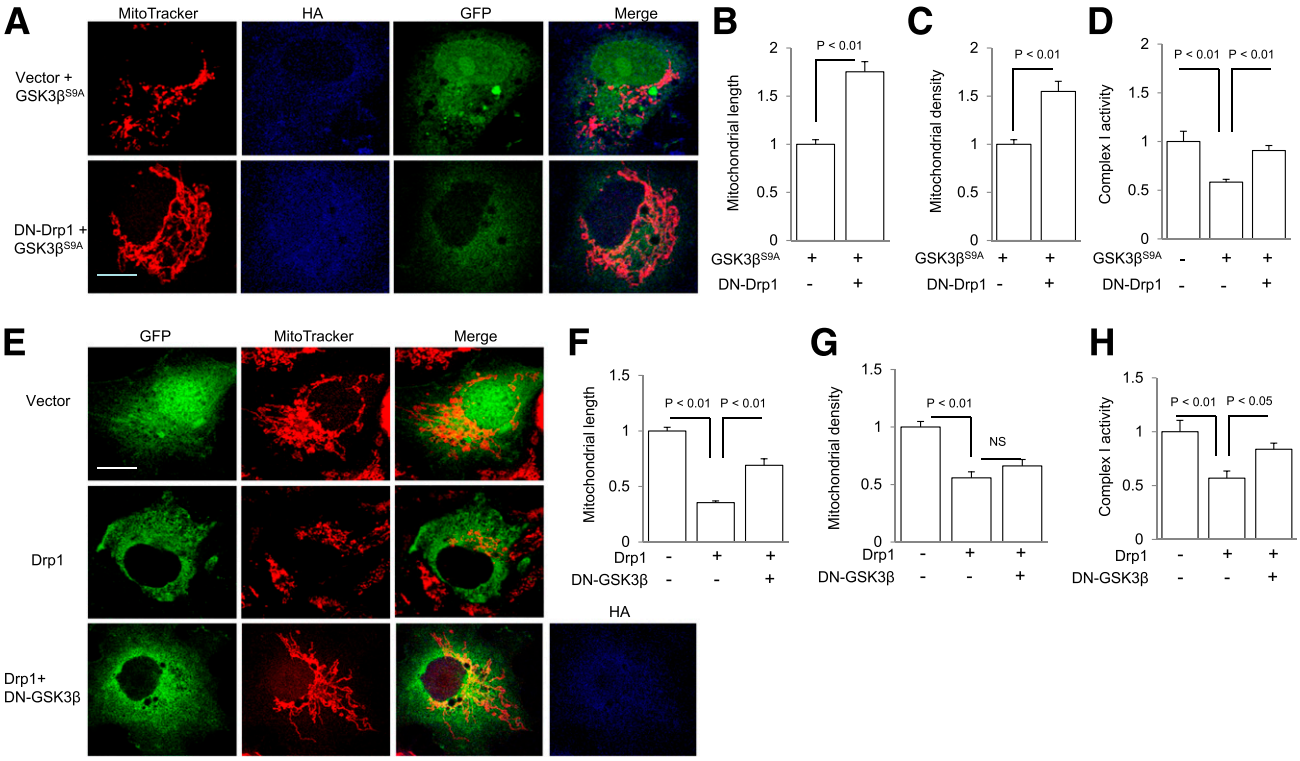

Figure 5—Effect of GSK3β on Drp1-induced mitochondrial morphology and function. *A*: Representative images showing MitoTracker red staining in cells cotransfected with GFP empty vector (green) and HA-GSK3β^{S9A} (HA-tagged GSK3β^{S9A} [blue]) (upper panel) or with DN-Drp1 (GFP-tagged Drp1^{K38A} [green]) and HA-GSK3β^{S9A} (blue) (bottom panel), respectively. GFP (green) and HA (blue) costaining showed cotransfection with both DN-Drp1 (or GFP empty vector) and GSK3β^{S9A} plasmids (HA-positive staining). *B–D*: Measurement of mitochondrial length (*B*), density (*C*), or complex I enzyme activity (*D*) in the indicated groups of cells. *E*: Representative images for GFP (green), MitoTracker red, and HA (blue) staining of cells transfected with GFP vector (upper panel), Drp1 (GFP-tagged wild-type Drp1 [middle panel]), or Drp1 (GFP-tagged wild-type Drp1) with DN-GSK3β (HA-tagged) constructs (lower panel). Cells with both GFP and HA-positive staining were cotransfected with both Drp1 and DN-GSK3β plasmids. *F–H*: Measurement of mitochondrial length (*F*), density (*G*), or complex I enzyme activity (*H*) among indicated groups. $N \geq 20$ cells per group from two independent experiments. Scale bar = 10 μm. (-) Indicates the vector transfection and (+) indicates the presence of the indicated plasmid transfection.

(Fig. 7*I–K*) without changing basal synaptic function in *db/m* hippocampus. Since insulin (19) and corticosterone (8) signaling pathways were reported to mediate LTP impairment in rodent models of diabetes, we explored their reaction to mdivi-1 treatment. Consistent with the previous report (8,19), we did find increased blood levels of insulin and corticosterone ($P < 0.05$ vs. *db/m*) in *db/db* mice (Supplementary Fig. 6*A* and *B*). Mdivi-1 treatment did not significantly change insulin and corticosterone levels ($P > 0.05$) (Supplementary Fig. 6*A* and *B*) or blood glucose content in control or *db/db* mice (Supplementary Table 1). These findings suggest that the protective effect of mdivi-1 on LTP restoration in diabetic hippocampus is not likely due to insulin or corticosterone signaling pathways.

DISCUSSION

In the current study, we report a novel and pivotal role of mitochondrial dysfunction in diabetes-induced synaptic impairment. Our data suggest a GSK3β/Drp1-dependent connection between mitochondrial dysfunction in diabetic neurons and LTP deficit. We believe that such a link is rational because provision of neurons with access to energy/metabolism homeostasis is the prerequisite for synaptic transmission. Understanding mitochondrial alterations in animal models of diabetes will likely generate novel approaches for the treatment of diabetes-associated neurological disorders.

Perturbations in maintenance of mitochondrial morphology and function are involved in several adverse effects of diabetes in many organs including pancreas (26,32), liver (27), skeletal muscle (9,28), and the vascular system (29,30). Brain is highly enriched with mitochondria and strongly reliant on oxidative phosphorylation for energy production. The current literature suggests a connection between diabetes and mitochondrial biogenesis and fission within mouse dorsal root ganglia (15,31). One of our recent publications suggests that mitochondrial dysfunction is associated with synaptic deficit in an Alzheimer disease mouse model superimposed with type 1 diabetes (36). However, it is still unclear whether dysfunctional synaptic plasticity (resulting in observed episodic memory impairment) links to mitochondrial defects in type 2 diabetes.

Staining of *db/db* mouse hippocampal pyramidal neurons for the mitochondrial marker SODII or COXIV

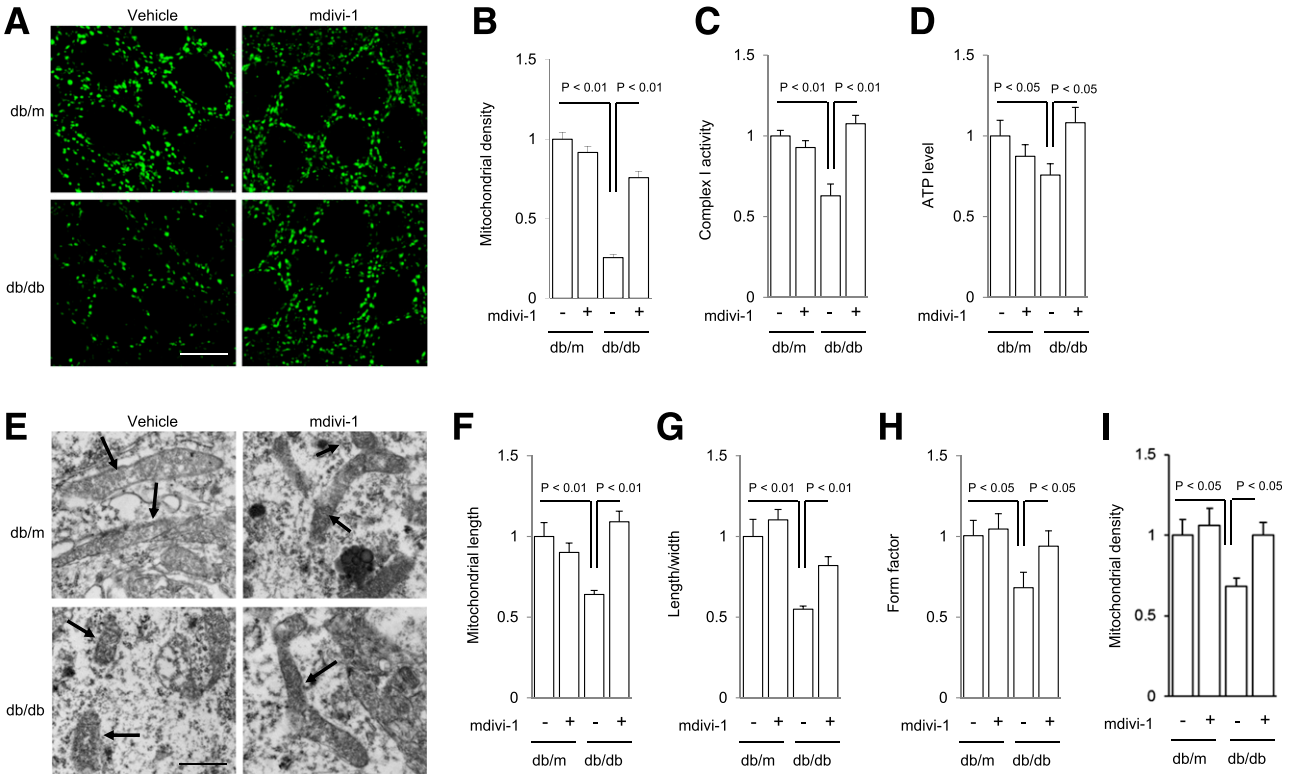

Figure 6—Effect of Drp1 inhibitor mdivi-1 on mitochondrial changes in diabetic hippocampus. *A*: Representative images of SODII staining of hippocampal neurons from the indicated groups using confocal microscopy. Scale bar = 10 μm. *B–D*: Quantification of mitochondrial density using MetaMorph software (*B*), complex I activity (*C*), and ATP levels (*D*) in the indicated groups of animals treated with vehicle (-) or mdivi-1 (+). Data are presented as fold increase relative to vehicle-treated *db/m* mice of indicated hippocampi. *E*: Representative electron microscope images of mitochondria (indicated by arrows). Scale bar = 500 nm. *F–H*: Quantification of mitochondrial length (*F*), ratio of length to width (*G*), form factor (*H*), and mitochondrial density (*I*) in the indicated groups of animals treated with vehicle (-) or mdivi-1 (+) from electron microscope images. *N* = 6–11 animals per group.

revealed a significant reduction of mitochondria compared with control(s). This reduction in neuronal mitochondria is suggestive of a diabetes-mediated interference with mitochondrial biogenesis and fission. In addition, these mitochondrial morphology changes were confirmed by electron microscopy. Measurement of hippocampal mitochondrial functional capacity in this mouse model of diabetes indicated significantly reduced activity of mitochondrial respiration complex I and lowered ATP content. Our results are consistent with findings of a similar study probing the skeletal muscle of patients with type 2 diabetes (33), in which there are impairments in energy metabolism and respiratory complex enzyme activity. Balance of mitochondrial fission and fusion processes is crucial for maintenance of mitochondrial morphology and function (59,60). In diabetic hippocampus, the mitochondrial fission protein, Drp1, was significantly increased and its phosphorylation was coincidentally elevated. On the other hand, levels of Mfn2, OPA1, and other auxiliary mitochondrial proteins such as HSP60 (data not shown) were not altered in diabetic hippocampus. Our findings are consistent with previous investigations of diabetic neuropathy, which included reports of increased Drp1 expression and mitochondrial fission in dorsal root ganglion neurons of 6-month-old *db/db* mice (15,31). In contrast to the greater numbers of mitochondria in dorsal root ganglion neurons (31), we note that hippocampal neurons in 5- to 6-month-old *db/db* mice displayed smaller numbers of mitochondria, while there was no sign showing mitochondrial decline among subjects younger than 3 months (data not shown). Differences in sensitivity to hyperglycemia between hippocampal neurons and dorsal root ganglion cells may account for the differences in our findings compared with previous studies (31). In addition, increased mitochondrial fission may eventually result in mitochondrial degeneration if the balance of fission and fusion is not maintained. We further tested whether mitochondrial enzyme (COXI) activity and ATP content were changed at 3 months and 6 months of age. We found that complex I enzyme activity significantly declined by 15% and 35% at 3 and 6 months of ages, respectively, though no significant alteration in ATP content was found at 3 months of age (Supplementary Fig. 7*A* and *B*). Similarly, the LTP significantly declined by 16% in 3-month-old *db/db* hippocampus compared with that of age-matched *db/m* control mice (Supplementary Fig. 7*C–E*). These data suggest age-dependent defects in mitochondrial and synaptic function. Pharmacologic or

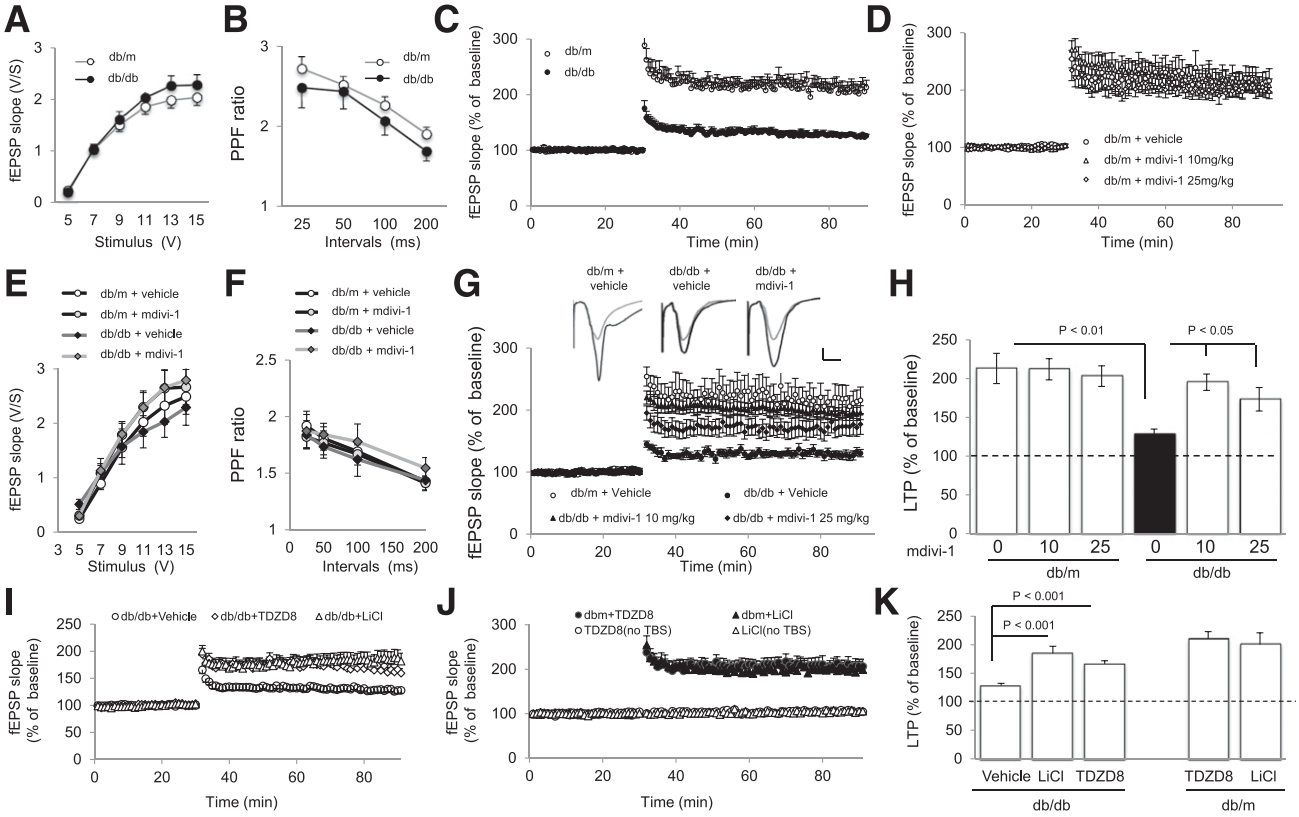

Figure 7—Effect of Drp1 inhibitor mdivi-1 or GSK3β inhibition on diabetes-impaired LTP in hippocampal CA1 region. *A* and *B*: Basal synaptic transmission (*A*) and paired-pulse facilitation (PPF) (*B*) were not significantly affected by diabetes. *C*: Hippocampal LTP is significantly lower in *db/db* mice compared with *db/m* control slices. *D–F*: Hippocampal LTP (*D*), basal synaptic transmission (*E*), and paired-pulse facilitation (*F*) in *db/m* mouse brain administered with vehicle or mdivi-1 (10 and 25 mg/kg i.p injection daily for 2 weeks) were similar. *G*: Diabetes-impaired hippocampal LTP was restored by mdivi-1 administration. Upper panel is representative of fEPSP traces indicating the neurotransmission responses before (gray) and after (black) θ-burst stimulation from mdivi-1–treated/nontreated animals. Vertical bar = 1 mV, horizontal bar = 5 ms. *H*: LTP levels of indicated animal groups were calculated by averaging the last 10 min of fEPSP slope. *I–K*: Blocking GSK3β activation with TDZD8 (5 μmol/L) or LiCl (4 mmol/L) suppressed LTP reduction in *db/db* hippocampus (*I*) but did not change the baseline or the LTP levels in *db/m* controls (*J*). LTP levels of indicated animal groups were calculated by averaging the last 10 min of fEPSP slope and are illustrated in *K*. TBS, θ-burst stimulation. Dashed lines in *H* and *K* indicate the baseline level. TBS, θ-burst stimulation; V/S, voltage/second. *N* = 8–14 slices of 5–8 animals per group.

genetic inactivation of Drp1 significantly prevented mitochondrial morphology and function changes in *db/db* hippocampus or human SK cells under high-glucose conditions, indicating a role of Drp1 in diabetes-induced mitochondrial morphology and functional changes.

There is at least one mechanism by which diabetes elevates Drp1 expression and phosphorylation resulting in mitochondrial alterations. To our knowledge, Drp1 is able to be phosphorylated at several sites by different kinases. It was first identified that Drp1 can be phosphorylated at Ser^{637} by protein kinase A (61,62), which was coincident with mitochondrial elongation. CaMK I can also phosphorylate the Ser^{637} site to promote mitochondrial fission (63). While the role of phosphorylated Drp1 at the Ser^{616} site still remains paradoxical, increasing evidence points out that Ser^{616} Drp1 is related to the mitochondrial fragmentation; for example, cyclin-dependent kinase 1/cyclin B–dependent phosphorylation at Ser^{616} of Drp1 induced mitochondrial fission during mitosis (64). Furthermore, our recent studies suggest a role of extracellular signal–related kinase 1/2 in oxidative stress–induced increased phosphorylation of Drp1 (37). In our present study, we observed mitochondrial degeneration/fragmentation along with elevated levels of Drp1 phosphorylation at Ser^{616} in diabetic conditions both in vivo and in vitro. GSK3β is activated in *db/db* mice in vivo owing to dephosphorylation on Ser^{9} residue (48,49) and can use Drp1 as one of its substrates in in vitro systems (51–53). We therefore focused on the role of GSK3β-mediated mitochondrial defects by modulating Drp1 Ser^{616} phosphorylation. We have clearly demonstrated that GSK3β activation was elevated in either type 2 diabetes–affected hippocampus or high glucose–treated human neuronal cell lines. While the underlying mechanisms for the alterations in GSK3β activation in in vivo and in vitro diabetic conditions are not clear, diabetes-induced Akt dephosphorylation (Supplementary Fig. 8*A* and *B*) may contribute, at least in part, to the GSK3β activation in addition to the aforementioned activation of other kinases. Indeed, we observe that pharmacological

inhibition of GSK3β successfully prevented Drp1 phosphorylation at Ser^{616} in the diabetes-affected mouse brain and high glucose–treated human cell line. These results further support the role of GSK3β in diabetes-induced mitochondrial defects via Drp1-mediated abnormal mitochondrial fission, though our results would not exclude the possibility of the involvement of extracellular signal-regulated kinases 1/2 in high glucose–induced Drp1 Ser^{616} phosphorylation and mitochondrial fragmentation (65). Furthermore, we demonstrated that genetic activation of GSK3β without high-glucose treatment can also promote mitochondrial fragmentation. The inactivation of GSK3β prevents high glucose–induced mitochondrial alterations. Taken together, these data suggest that GSK3β is one of the mechanisms underlying diabetes-induced mitochondrial abnormalities.

GSK3β most likely acts as an upstream signaling mechanism for Drp1 upregulation in diabetes-induced mitochondrial dysfunction. Phosphorylation of Ser^{9} on GSK3β in *db/db* hippocampus was decreased, resulting in higher levels of the active form of GSK3β. Inhibition of GSK3β activity was associated with suppressed phosphorylation of Ser^{616} on Drp1, a critical step enabling Drp1 GTPase activity for mitochondrial fission (46). Currently, there are no inhibitors available for prevention of Drp1 Ser^{616} phosphorylation; however, treatment with mdivi-1 (inhibiting the GTPase activity of Drp1) maintained mitochondrial morphology and function, though GSK3β activation was unaltered. GSK3β not only acts as an upstream signaling mechanism for Drp1 but also directly interacts with Drp1, which, in turn, is responsible for phosphorylation of Drp1 Ser^{693} and leads to decreased GTPase activity and an enhancement of mitochondrial fusion/elongation (53). We also determined whether an inactive form of GSK3β (p-ser9 GSK3β) interacts with Drp1. We found that pull-down GSK3β (active form) yielded Drp1 immunoreaction bands in *db/db* animals, but no interaction was found between p-ser9 GSK3β and Drp1 (data not shown).

Using a human neuronal cell line, we directly modulated GSK3β or Drp1 activation by transfection with different targeted vectors. Inactivation of GSK3β prevented GSK3β-involved activation of Drp1 signaling and changes in mitochondrial morphology and function under diabetic conditions. However, inactivation of Drp1 did not alter GSK3β activation even though it preserved mitochondrial morphology under high-glucose conditions, suggesting a role for GSK3β in diabetes-induced activation of Drp1 signaling involved in alterations in mitochondrial morphology.

Another major novel finding of the current study is that diabetes-induced synaptic transmission deficit, at least in part, depends on GSK3β/Drp1-mediated mitochondrial abnormalities. Consistent with the results of other researchers (5,7,8,11,16–20), we observed LTP reduction in the hippocampal CA1 region in *db/db* mice. Because complete absence of Drp1 in mice is lethal, we were not able to generate diabetic *db/db* mice with Drp1 knocked out at this point; however, we successfully restored diabetes-induced mitochondrial alterations by treating mice with the Drp1 inhibitor, mdivi-1. Treatment with mdivi-1 restores mitochondrial function along with the improvement in LTP in the diabetic hippocampus. Notably, a recent investigation demonstrates that mdivi-1 also inhibits the rapidly activating delayed-rectifier potassium channel (66) in murine cardiomyocyte cell lines. While the inhibitory effect of mdivi-1 on potassium channels has not yet been tested in neurons, mdivi-1 might cause an elevated excitatory activity in the central nervous system if a potential effect on potassium ion channel exists. This requires further investigation. The beneficial effect of inhibiting Drp1-mediated aberrant mitochondrial and synaptic function by mdivi-1 treatment is unlikely owing to an insulin- or corticosterone-dependent mechanism (8). Indeed, corticosterone levels are increased in diabetic animals compared with nondiabetic littermates; however, inhibition of Drp1 using mdivi-1 failed to prevent diabetes-induced corticosterone increases but did ameliorate diabetes-induced hippocampal LTP deficits.

In summary, our study offers new insights into the role of GSK3β/Drp1 interaction in diabetes-induced mitochondrial and synaptic dysfunction. We clearly demonstrated alterations in mitochondrial structure and function in diabetes-affected hippocampus. Impaired structural or functional capacity of mitochondria is attributable to type 2 diabetes–induced impairment of synaptic plasticity. Inhibition of GSK3β/Drp1-mediated deficits in mitochondrial architecture and resultant functional changes ameliorate LTP deficit. Blockade of GSK3β activation or inhibition of mitochondrial division significantly improves mitochondrial and synaptic function under diabetic conditions. These studies suggest targets for the development of interventions to prevent or treat diabetes-induced mitochondrial deficits and accompanying neurodegeneration.

Funding. This study was supported by grants from the National Institute on Aging (R37AG037319 and R01AG044793) and National Institute of Neurological Disorders and Stroke (R01NS065482).

Duality of Interest. No potential conflicts of interest relevant to this article were reported.

Author Contributions. S.H., X.G., and D.F. performed experiments and statistical analysis. Y.W. supervised and analyzed all the experimental data, wrote the manuscript, and performed experiments and statistical analysis. C.Z. and L.W. performed experiments. G.H. prepared constructs. A.A.S. and G.M.M. conducted electron microscope experiments. H.Y. performed statistical analysis. S.S.Y. directed, designed, and supervised this study and wrote the manuscript. S.S.Y. is the guarantor of this work and, as such, had full access to all the data in the study and takes responsibility for the integrity of the data and the accuracy of the data analysis.

References

1. Schmidt RE, Parvin CA, Green KG. Synaptic ultrastructural alterations anticipate the development of neuroaxonal dystrophy in sympathetic ganglia of aged and diabetic mice. J Neuropathol Exp Neurol 2008;67:1166–1186

2. Tay SS, Wong WC. Ultrastructural changes in the gracile nucleus of alloxan-induced diabetic rats. Acta Anat (Basel) 1990;139:367–373

3. Greenwood CE, Winocur G. High-fat diets, insulin resistance and declining cognitive function. Neurobiol Aging 2005;26(Suppl. 1):42–45

4. Desrocher M, Rovet J. Neurocognitive correlates of type 1 diabetes mellitus in childhood. Child Neuropsychol 2004;10:36–52
5. Biessels GJ, Kamal A, Ramakers GM, et al. Place learning and hippocampal synaptic plasticity in streptozotocin-induced diabetic rats. Diabetes 1996;45: 1259–1266
6. Biessels GJ, Kamal A, Urban IJ, Spruijt BM, Erkelens DW, Gispen WH. Water maze learning and hippocampal synaptic plasticity in streptozotocin-diabetic rats: effects of insulin treatment. Brain Res 1998;800:125–135
7. Li XL, Aou S, Oomura Y, Hori N, Fukunaga K, Hori T. Impairment of long-term potentiation and spatial memory in leptin receptor-deficient rodents. Neuroscience 2002;113:607–615
8. Stranahan AM, Arumugam TV, Cutler RG, Lee K, Egan JM, Mattson MP. Diabetes impairs hippocampal function through glucocorticoid-mediated effects on new and mature neurons. Nat Neurosci 2008;11:309–317
9. Zorzano A, Liesa M, Palacín M. Role of mitochondrial dynamics proteins in the pathophysiology of obesity and type 2 diabetes. Int J Biochem Cell Biol 2009; 41:1846–1854
10. Yoon Y, Galloway CA, Jhun BS, Yu T. Mitochondrial dynamics in diabetes. Antioxid Redox Signal 2011;14:439–457
11. Stranahan AM, Arumugam TV, Lee K, Mattson MP. Mineralocorticoid receptor activation restores medial perforant path LTP in diabetic rats. Synapse 2010;64:528–532
12. Messier C. Impact of impaired glucose tolerance and type 2 diabetes on cognitive aging. Neurobiol Aging 2005;26(Suppl. 1):26–30
13. Yaffe K, Lindquist K, Schwartz AV, et al. Advanced glycation end product level, diabetes, and accelerated cognitive aging. Neurology 2011;77:1351–1356
14. Yu T, Sheu SS, Robotham JL, Yoon Y. Mitochondrial fission mediates high glucose-induced cell death through elevated production of reactive oxygen species. Cardiovasc Res 2008;79:341–351
15. Edwards JL, Quattrini A, Lentz SI, et al. Diabetes regulates mitochondrial biogenesis and fission in mouse neurons. Diabetologia 2010;53:160–169
16. Abbas T, Faivre E, Hölscher C. Impairment of synaptic plasticity and memory formation in GLP-1 receptor KO mice: Interaction between type 2 diabetes and Alzheimer's disease. Behav Brain Res 2009;205:265–271
17. Artola A, Kamal A, Ramakers GM, Biessels GJ, Gispen WH. Diabetes mellitus concomitantly facilitates the induction of long-term depression and inhibits that of long-term potentiation in hippocampus. Eur J Neurosci 2005;22: 169–178
18. Martín ED, Sánchez-Perez A, Trejo JL, et al. IRS-2 deficiency impairs NMDA receptor-dependent long-term potentiation. Cereb Cortex 2012;22:1717–1727
19. Nisticò R, Cavallucci V, Piccinin S, et al. Insulin receptor β-subunit haploinsufficiency impairs hippocampal late-phase LTP and recognition memory. Neuromolecular Med 2012;14:262–269
20. Shonesy BC, Thiruchelvam K, Parameshwaran K, et al. Central insulin resistance and synaptic dysfunction in intracerebroventricular-streptozotocin injected rodents. Neurobiol Aging 2012;33:430.e5–430.e18
21. Reijmer YD, van den Berg E, Ruis C, Kappelle LJ, Biessels GJ. Cognitive dysfunction in patients with type 2 diabetes. Diabetes Metab Res Rev 2010;26: 507–519
22. Brands AM, Biessels GJ, de Haan EH, Kappelle LJ, Kessels RP. The effects of type 1 diabetes on cognitive performance: a meta-analysis. Diabetes Care 2005;28:726–735
23. Kageyama Y, Zhang Z, Sesaki H. Mitochondrial division: molecular machinery and physiological functions. Curr Opin Cell Biol 2011;23:427–434
24. Palmer CS, Osellame LD, Stojanovski D, Ryan MT. The regulation of mitochondrial morphology: intricate mechanisms and dynamic machinery. Cell Signal 2011;23:1534–1545
25. Reddy PH, Reddy TP, Manczak M, Calkins MJ, Shirendeb U, Mao P. Dynamin-related protein 1 and mitochondrial fragmentation in neurodegenerative diseases. Brain Res Brain Res Rev 2011;67:103–118
26. Molina AJ, Wikstrom JD, Stiles L, et al. Mitochondrial networking protects beta-cells from nutrient-induced apoptosis. Diabetes 2009;58:2303–2315
27. Yu T, Robotham JL, Yoon Y. Increased production of reactive oxygen species in hyperglycemic conditions requires dynamic change of mitochondrial morphology. Proc Natl Acad Sci U S A 2006;103:2653–2658
28. Bach D, Pich S, Soriano FX, et al. Mitofusin-2 determines mitochondrial network architecture and mitochondrial metabolism. A novel regulatory mechanism altered in obesity. J Biol Chem 2003;278:17190–17197
29. Widlansky ME, Wang J, Shenouda SM, et al. Altered mitochondrial membrane potential, mass, and morphology in the mononuclear cells of humans with type 2 diabetes. Transl Res 2010;156:15–25
30. Makino A, Scott BT, Dillmann WH. Mitochondrial fragmentation and superoxide anion production in coronary endothelial cells from a mouse model of type 1 diabetes. Diabetologia 2010;53:1783–1794
31. Vincent AM, Edwards JL, McLean LL, et al. Mitochondrial biogenesis and fission in axons in cell culture and animal models of diabetic neuropathy. Acta Neuropathol 2010;120:477–489
32. Lowell BB, Shulman GI. Mitochondrial dysfunction and type 2 diabetes. Science 2005;307:384–387
33. Kelley DE, He J, Menshikova EV, Ritov VB. Dysfunction of mitochondria in human skeletal muscle in type 2 diabetes. Diabetes 2002;51:2944–2950
34. Chen H, Charlat O, Tartaglia LA, et al. Evidence that the diabetes gene encodes the leptin receptor: identification of a mutation in the leptin receptor gene in db/db mice. Cell 1996;84:491–495
35. Du H, Guo L, Fang F, et al. Cyclophilin D deficiency attenuates mitochondrial and neuronal perturbation and ameliorates learning and memory in Alzheimer's disease. Nat Med 2008;14:1097–1105
36. Wang Y, Wu L, Fang D, et al. Synergistic exacerbation of mitochondrial and synaptic dysfunction and resultant learning and memory deficit in a mouse model of diabetic Alzheimer's disease. J Alzheimers Dis 2015;43: 451–463
37. Gan X, Huang S, Wu L, et al. Inhibition of ERK-DLP1 signaling and mitochondrial division alleviates mitochondrial dysfunction in Alzheimer's disease cybrid cell. Biochim Biophys Acta 2013;1842:220–231
38. Lustbader JW, Cirilli M, Lin C, et al. ABAD directly links Abeta to mitochondrial toxicity in Alzheimer's disease. Science 2004;304:448–452
39. Tieu K, Perier C, Caspersen C, et al. D-beta-hydroxybutyrate rescues mitochondrial respiration and mitigates features of Parkinson disease. J Clin Invest 2003;112:892–901
40. Xu H, Wu ZY, Fang F, et al. Genetic deficiency of Irgm1 (LRG-47) suppresses induction of experimental autoimmune encephalomyelitis by promoting apoptosis of activated CD4+ T cells. FASEB J 2010;24:1583–1592
41. Winer J, Jung CK, Shackel I, Williams PM. Development and validation of real-time quantitative reverse transcriptase-polymerase chain reaction for monitoring gene expression in cardiac myocytes in vitro. Anal Biochem 1999;270:41–49
42. Jheng HF, Tsai PJ, Guo SM, et al. Mitochondrial fission contributes to mitochondrial dysfunction and insulin resistance in skeletal muscle. Mol Cell Biol 2012;32:309–319
43. Gawlowski T, Suarez J, Scott B, et al. Modulation of dynamin-related protein 1 (DRP1) function by increased O-linked-β-N-acetylglucosamine modification (O-GlcNAc) in cardiac myocytes. J Biol Chem 2012;287:30024–30034
44. Shenouda SM, Widlansky ME, Chen K, et al. Altered mitochondrial dynamics contributes to endothelial dysfunction in diabetes mellitus. Circulation 2011;124: 444–453
45. Men X, Wang H, Li M, et al. Dynamin-related protein 1 mediates high glucose induced pancreatic beta cell apoptosis. Int J Biochem Cell Biol 2009;41:879–890
46. Kashatus DF, Lim KH, Brady DC, Pershing NL, Cox AD, Counter CM. RALA and RALBP1 regulate mitochondrial fission at mitosis. Nat Cell Biol 2011;13:1108–1115
47. Cassidy-Stone A, Chipuk JE, Ingerman E, et al. Chemical inhibition of the mitochondrial division dynamin reveals its role in Bax/Bak-dependent mitochondrial outer membrane permeabilization. Dev Cell 2008;14:193–204
48. Wang Y, Feng W, Xue W, et al. Inactivation of GSK-3beta by metallothionein prevents diabetes-related changes in cardiac energy metabolism, inflammation, nitrosative damage, and remodeling. Diabetes 2009;58:1391–1402

49. Shuai H, Zhang J, Zhang J, et al. Role of stereotaxically injected IgG from db/db mice in the phosphorylation of the microtubule-associated protein tau in hippocampus. Brain Res 2012;1486:14–26
50. Cross DA, Alessi DR, Cohen P, Andjelkovich M, Hemmings BA. Inhibition of glycogen synthase kinase-3 by insulin mediated by protein kinase B. Nature 1995;378:785–789
51. Chen CH, Hwang SL, Howng SL, Chou CK, Hong YR. Three rat brain alternative splicing dynamin-like protein variants: interaction with the glycogen synthase kinase 3beta and action as a substrate. Biochem Biophys Res Commun 2000;268:893–898
52. Hong YR, Chen CH, Cheng DS, Howng SL, Chow CC. Human dynamin-like protein interacts with the glycogen synthase kinase 3beta. Biochem Biophys Res Commun 1998;249:697–703
53. Chou CH, Lin CC, Yang MC, et al. GSK3beta-mediated Drp1 phosphorylation induced elongated mitochondrial morphology against oxidative stress. PLoS ONE 2012;7:e49112
54. Martinez A, Alonso M, Castro A, Pérez C, Moreno FJ. First non-ATP competitive glycogen synthase kinase 3 beta (GSK-3beta) inhibitors: thiadiazolidinones (TDZD) as potential drugs for the treatment of Alzheimer's disease. J Med Chem 2002;45:1292–1299
55. Kimura R, Ma LY, Wu C, et al. Acute exposure to the mitochondrial complex I toxin rotenone impairs synaptic long-term potentiation in rat hippocampal slices. CNS Neurosci Ther 2012;18:641–646
56. Kim HY, Lee KY, Lu Y, et al. Mitochondrial Ca(2+) uptake is essential for synaptic plasticity in pain. J Neurosci 2011;31:12982–12991
57. Mattson MP, Gleichmann M, Cheng A. Mitochondria in neuroplasticity and neurological disorders. Neuron 2008;60:748–766
58. Levy M, Faas GC, Saggau P, Craigen WJ, Sweatt JD. Mitochondrial regulation of synaptic plasticity in the hippocampus. J Biol Chem 2003;278:17727–17734
59. Chan DC. Mitochondria: dynamic organelles in disease, aging, and development. Cell 2006;125:1241–1252
60. Chan DC. Mitochondrial fusion and fission in mammals. Annu Rev Cell Dev Biol 2006;22:79–99
61. Cribbs JT, Strack S. Reversible phosphorylation of Drp1 by cyclic AMP-dependent protein kinase and calcineurin regulates mitochondrial fission and cell death. EMBO Rep 2007;8:939–944
62. Chang CR, Blackstone C. Cyclic AMP-dependent protein kinase phosphorylation of Drp1 regulates its GTPase activity and mitochondrial morphology. J Biol Chem 2007;282:21583–21587
63. Han XJ, Lu YF, Li SA, et al. CaM kinase I alpha-induced phosphorylation of Drp1 regulates mitochondrial morphology. J Cell Biol 2008;182:573–585
64. Taguchi N, Ishihara N, Jofuku A, Oka T, Mihara K. Mitotic phosphorylation of dynamin-related GTPase Drp1 participates in mitochondrial fission. J Biol Chem 2007;282:11521–11529
65. Yu T, Jhun BS, Yoon Y. High-glucose stimulation increases reactive oxygen species production through the calcium and mitogen-activated protein kinase-mediated activation of mitochondrial fission. Antioxid Redox Signal 2011;14:425–437
66. So EC, Hsing CH, Liang CH, Wu SN. The actions of mdivi-1, an inhibitor of mitochondrial fission, on rapidly activating delayed-rectifier K^+ current and membrane potential in HL-1 murine atrial cardiomyocytes. Eur J Pharmacol 2012;683:1–9